Energy Conversion and Management 81 (2014) 41–50

Contents lists available at ScienceDirect

Energy Conversion and Management

journal homepage: www.elsevier.com/locate/enconman

Numerical investigation of biogas flameless combustion

Seyed Ehsan Hosseini *, Ghobad Bagheri, Mazlan Abdul Wahid

High-Speed Reacting Flow Laboratory, Faculty of Mechanical Engineering, Universiti Teknologi Malaysia, 81310 UTM Skudai, Johor, Malaysia

ARTICLE INFO

Article history:
Received 27 September 2013
Accepted 3 February 2014
Available online 3 March 2014

Keywords:
Biogas
Flameless combustion
Simulation
Entropy
Fuel consumption
Pollutant formation

ABSTRACT

The purpose of this investigation is to analyze combustion characteristics of biogas flameless mode based on clean technology development strategies. A three dimensional (3D) computational fluid dynamic (CFD) study has been performed to illustrate various priorities of biogas flameless combustion compared to the conventional mode. The effects of preheated temperature and wall temperature, reaction zone and pollutant formation are observed and the impacts of combustion and turbulence models on numerical results are discussed. Although preheated conventional combustion could be effective in terms of fuel consumption reduction, NO_x formation increases. It has been found that biogas is not eligible to be applied in furnace heat up due to its low calorific value (LCV) and it is necessary to utilize a high calorific value fuel to preheat the furnace. The required enthalpy for biogas auto-ignition temperature is supplied by enthalpy of preheated oxidizer. In biogas flameless combustion, the mean temperature of the furnace is lower than traditional combustion throughout the chamber. Compared to the biogas flameless combustion with uniform temperature, very high and fluctuated temperatures are recorded in conventional combustion. Since high entropy generation intensifies irreversibility, exergy loss is higher in biogas conventional combustion compared to the biogas flameless regime. Entropy generation minimization in flameless mode is attributed to the uniform temperature inside the chamber.

1. Introduction

Industrial development is in debt of energy consumption and more than 80% of the world energy demand is supplied by different kinds of fossil fuels. However, the resources of fossil fuels are depleted day by day and the future energy scenario of the world has become one of the main concerns. Indeed, environmental concerns have increased due to raising rate of emissions released from fossil fuel combustion. Global warming (GW) has become one of the most important environmental issues due to increasing rate of greenhouse gases (GHGs) generation. Therefore, the request for clean alternative fuel and efficient combustion technology has become more important [1–3]. In recent decades, utilization of renewable and sustainable energy such as biomass, solar energy, wind energy, hydropower and geothermal has been developed properly. Furthermore, biogas from wastewater effluent, municipal solid wastes (MSW), animal waste and agricultural by-products have been employed for combined heat and power (CHP) generation purposes [4–8]. In the other hand, necessity of biogas collection from aforementioned resources is unavoidable because CH_4 and CO_2 as the main components of biogas participate in the GW constitution actively [9]. Since the negative effect of CH_4 on the GW is 23 times more than CO_2, biogas collection from anaerobic digestion (AD) has become more highlighted. In most of the AD, the percentage of CH_4 is enough to be considered as a clean fuel. The amount of CH_4 in biogas components depends on the feedstock is various (from 40% up to 60%) [10]. In biogas conventional combustion, pollutant formation mitigates compared to traditional combustion of pure CH_4. However, biogas traditional combustion encounters some problems due to LCV of biogas. Therefore, biogas should be upgraded to remove its non-combustible CO_2 impurity [11]. Based on the application of biogas, pure biogas can be cleaned and upgraded by some technologies such as water scrubbing, cryogenic process and membrane. In order to prevent implementation of upgrading equipment, application of flameless combustion was proposed for pure biogas combustion. Since combustion is still the most important technique for energy generation, flameless combustion was introduced to improve the combustion efficiency and decrease pollutant formation concomitantly [12,13]. The importance of flameless combustion technology has become more highlighted when the inability of other combustion technologies in terms of simultaneous pollutant reduction and thermal efficiency enhancement was proven. Low emission formation in flameless combustion is obtained due to dilution of the air combustion by inert gases such as nitrogen (N_2) and CO_2 [14–16]. Therefore,

* Corresponding author. Tel.: +60 1112600959.
E-mail address: seyed.ehsan.hosseini@gmail.com (S.E. Hosseini).

http://dx.doi.org/10.1016/j.enconman.2014.02.006
0196-8904/

Nomenclature

$\vec{r}$	position vector	$T_{s,o}$	outer surface temperature
$\vec{s}$	direction vector	T_∞	the ambient temperature set at 300°K
I	radiation intensity	h	natural convection coefficient
I_λ	radiation intensity for wavelength λ	σ	Stephane-Boltzmann constant (5.67×10^{-8} W/m^2 K^4)
a_λ	spectral absorption coefficient	ε	solid surface emissivity
$I_{b\lambda}$	black body intensity	x	percentage of excess air
$\vec{s}'$	scattering direction vector	β	mole fraction of CO_2 in biogas
s	path length	r	density (Kg/m^3)
n	refractive index	k_f	thermal conductivity of fluid
σ_s	scattering coefficient	Y_i	mass fraction of species i
σ	Stephan-Boltzmann constant (5.669×10^{-8} W/m^2 K^4)	W_i	generation or consumption of specious
Φ	phase function		
Ω'	solid angle		

combustion instability can be appeared due to low amounts of oxidizer and consequently flame quenching occurs. Thus the high temperature of diluted oxidizer plays an important role to exceed the auto – ignition temperature of the fuel. It can be construed that required enthalpy is supplied by preheating the oxidizer to achieve the self-ignition temperature of the fuel [17]. Although the great performance of flameless combustion has been developed in terms of fossil fuel utilization, various aspects of biogas flameless combustion have not been investigated properly. Since computational analyses are becoming more important due to their acceptable accuracy and lower cost, different perspectives of biogas flameless combustion can be analyzed numerically. The theoretical study using CFD software decreases errors and trials on experimental investigations for development of new models. In this article, a CFD modeling of biogas flameless combustion is investigated to identify the most important parameters that should be considered in biogas flameless regime. The effects of chemical kinetic mechanisms, turbulence models, radiation heat transfer and differential diffusion effects on the accuracy of the model are noted.

2. Conventional combustion of LCV fuels

One of the most important barriers for biogas utilization development is its low calorific value as well as its corrosive nature. LCV fuels were not taken into account in the energy mix of the world due to the abundance of high calorific value fossil fuels and lower energy prices in the past. However, recent enhancements of energy prices and concerns of the future energy scenario have attracted more attention to LCV fuel utilization in power generation. Therefore, combustion characteristics of various combinations of biogas have become more important. It has been claimed that raw biogas cannot be utilized in commercial burners directly as the substitution of natural gas (NG) or liquid petroleum gas (LPG). If biogas conducted to the traditional burner orifice at the pressure intended for charging NG or LPG, the air fuel ratio is not sufficient for combustion stability due to high CO_2 content of biogas. Thus, a new burner with the separate control measurement system should be installed for biogas. Since water vapor and H_2S as the components of biogas have corrosive characteristics, the condensation should be prevented by maintaining the furnace temperatures above the dew point temperature. It means that the combustion furnace should be heated up by NG or LPG to obtain higher operating temperature [18]. Therefore, a dual role burner should be installed in conventional combustion system fueled by biogas. Indeed, in order to switch over from NG or LPG to biogas some equipment should be employed. Consequently, complicated setting and the low efficiency of the conventional combustion systems can encourage biogas users to apply flameless combustion in their combustion process [19].

3. Numerical studies of flameless regime

Flameless combustion has been referred as flameless oxidation, colorless distributed combustion, moderate or intense low oxygen dilution (MILD) combustion and high-temperature air combustion (HiTac) [20]. In the flameless mode, combustion takes place in a distributed reaction zone with uniform low temperature. The fluctuations of temperature are omitted in flameless regime compared to the conventional flames. Combustion occurs in a low oxygen concentration atmosphere without visible flame. Indeed, the levels of the noise, NO_x and soot emissions decrease [21]. Due to complicated conditions in flameless mode, numerical modeling of the flameless regime has received especial attention. Weber et al. [22] modeled an industrial chamber with square cross section in steady state flameless combustion condition. Very high momentum oxidizer was charged through a central hole, NG was entered to the furnace through two injectors as a fuel and exhaust gases were recirculated in the system. In these circumstances, turbulence was modeled by standard k–ε model [23,24] and RNG k–ε model [25]. The combustion model was simulated with the eddy breakup model and a two-step reaction scheme; the eddy dissipation model (EDM) with the chemical equilibrium and the conserved scalar/prescribed probability density function (pdf) with a chemical equilibrium assumption. A similar numerical investigation was done by Kim et al. [26] who applied the standard k–ε model, the eddy-dissipation concept (EDC) and four different global reaction mechanisms. The characteristics of the MILD combustion system included a burner with a central fuel jet surrounded by six oxidizer jets and exhaust gases recirculation system was investigated numerically using k–ε and flamelet model by Coelho and Peters et al. [27] and Dally et al. [28]. It was pointed out that the numerical temperatures along the centerline of combustor were in good agreement with experimental records for pure CH_4 and CH_4 diluted with CO_2, and in poor agreement for CH_4 diluted with N_2. Khoshhal et al. [29] investigated NO_x formation and heat transfer mechanisms in a high temperature air combustion boiler numerically. It was pointed out that the experimental measured values and the CFD results illustrated good agreement. Although the temperatures of preheated oxidizer in flameless combustion mode are higher than conventional conditions, the reaction-controlling temperatures are lower than traditional combustion due to the low oxygen concentration. In the other hand, burner configuration is very important to achieve flameless conditions. In some investigations, burner contains a central inlet jet of fuel and some

inlet preheated air jets located around the central jet [30]. Also, the high-momentum preheated oxidizer can be conducted from the central of the burner surrounded by some low-momentum fuel jets [31]. The characteristics of the turbulent non-premixed methane/hydrogen flame issued by a jet in hot co-flow (JHC) were investigated numerically by Christo and Dally [32]. It was stipulated that differential diffusion effects should be considered in CFD modeling due to their crucial role in the accuracy of the calculations. Indeed, the numerical results of detailed chemical kinetics like the eddy dissipation concept (EDC) solver, illustrated higher accuracy in JHC. Galleti et al. [33] simulated a recuperative burner where the fuel was charged at the burner axis and the oxidizer was injected in a co-flow configuration. A flame tube with three windows was set to promote the internal recirculation of exhaust gases. Exhaust gas recirculation was done through those windows which mixed with the air before combustion. A modified standard k–ε model, a single one step mechanism and finite rate eddy dissipation method were considered in this study. Indeed, Parente et al. [34] studied NO_x formation in the aforementioned combustion system numerically. Various aspects of turbulence flameless models in high pressure gas turbine were investigated by Schütz et al. [35]. The premixed oxidizer and fuel were fed into the chamber via 12 nozzles located along a circle. Thanks to the mass continuity and very high velocity of the mixture, a recirculating annulus was formed around the nozzles. CFD simulation of the system was carried out either by GRI3.0 or by two-step global mechanism using k–ε method as the viscous model and EDC as the turbulence chemistry interaction model. Although, the numerical results were in good agreement with experimental records some shortcomings in the estimation of turbulence mixing were reported. In the other attempt, the characteristics of LCV gases combustion in a similar furnace operated at atmospheric temperature was simulated by Danon et al. [36]. Both realizable k–ε model and the Reynolds stress turbulence were applied in this modeling. An EDC model with two various chemical mechanisms were set. The differences between mean temperatures along the axis in numerical and experimental results were reported in the uncertainty range of the optimal. Chen and Zheng [37] investigated the effects of oxygen concentration, the temperature of oxidizer and the percentage of hydrogen on the hydrogen-enriched biogas counter-flow flameless combustion mathematically. It was pointed out hydrogen-enriched biogas flameless combustion can be sustained with low preheated temperature of the oxidizer and extremely highly diluted oxygen concentration in the oxidizer mixture. They applied flamelet approach for modeling the combustion and found an urgency to develop new turbulent combustion methods for flameless combustion.

Based on aforementioned literatures, it can be construed that the numerical simulation of the flameless combustion method is a challenging problem, due to the lack of comprehensive theoretical knowledge about this technique. Although excellent agreements between experimental and numerical investigations have sometimes been reported, few investigations were presented a holistic comparison of various turbulence and combustion models, chemical reaction mechanisms, and compared their numerical results with experimental data. Furthermore, a lack of comprehensive numerical investigation about biogas flameless combustion is observed due to complicated chemical reaction mechanism. Though the concept of fossil fuel flameless combustion has been extensively investigated numerically and mathematically, biogas flameless modeling has received little attention. Since low oxygen concentration of biogas flameless combustion has led the system to slower reaction rates and increase the effects of molecular diffusion on combustion characteristics, the applications of combustion models that presume fast chemistry and eliminate the impacts of differential diffusion are challenged [38].

4. CFD modeling

The CFD model of combustor designed for this numerical study is based on the geometry of the experimental lab-scale biogas flameless combustion carried out by Hosseini et al. [39]. The inside diameter and the length of the chamber are 150 mm and 600 mm respectively. The 5 mm central inlet of the burner is considered for biogas inlet and the other inlets are the oxidizer entrances. The exhaust gases are conducted to the outside of the chamber through a central hole with 50 mm diameter. Fig. 1 depicts the schematic of the biogas flameless furnace.

This 3D simulation is performed with ANSYS 14 using ANSYS Modeler to design the flameless furnace and ANSYS Meshing to mesh the furnace [40]. Convergence rate as well as scalar properties can be improved by mesh refinement and grid resolution for smooth flow representation can be ensured. The geometry of the furnace is not complicated in this numerical furnace model, therefore calculations speed increase due to mitigate meshing nodes and elements. The quantity of mesh grids directly impacts on the solution duration. Since the chamber model is symmetrical, just an eighth part of the model is solved. Fig. 2 demonstrates the meshes of the flameless chamber. To enhance the precision of predictions, the regions near the air and fuel nozzle have smaller control volume meshes.

The results of simulation with 7769 nodes and 33,798 elements is in good agreement with the experimental records. The grid independent of the simulation was tested by changing the number of nodes to the finer meshes. The number of elements were adopted 33,798, 68,453 and 100,356 to find the most conformity to the experimental records. However meaningful changes were not observed in the results and the grid independent of solution is

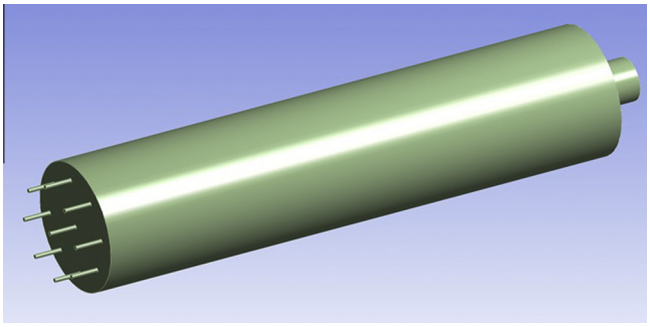

Fig. 1. Schematic of the flameless furnace.

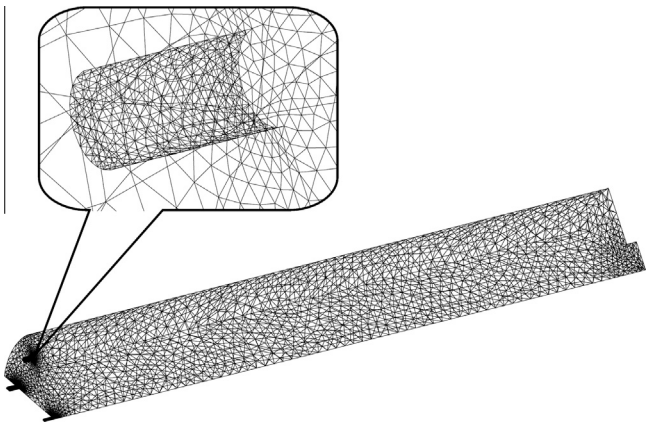

Fig. 2. An eighth part of the flameless furnace after meshing.

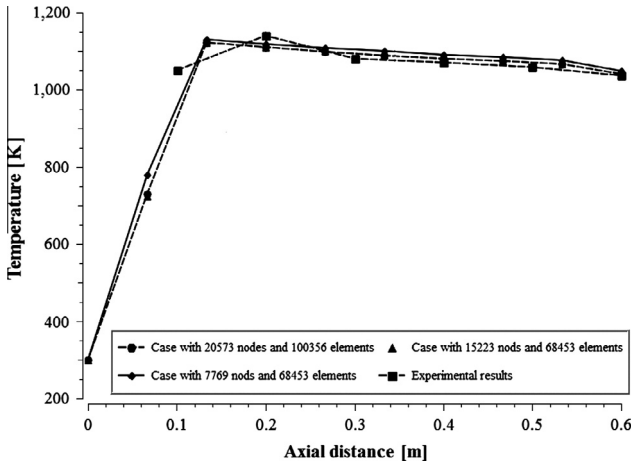

Fig. 3. The axial temperature variation of experimental and numerical results.

confirmed by this test. Fig. 3 shows the axial temperature variations of experimental and simulated data with respect to the various meshes when preheated air temperature was 900 K and the concentration of oxygen in the oxidizer was set 7%. This figure confirms that the experimental and simulated data have the same trend in terms of the temperature profile, and mesh with 7769 nodes was selected due to lower computational cost.

The governing equations (transport equations include continuity, energy, momentum) are solved using CFD package ANSYS FLUENT14 [40]. In Reynolds averaging, the variables in the exact Navier-Stoks equations are converted into he mean and fluctuating components. For all scalar quantities like energy, pressure and species concentration it can be written:

$$\emptyset = \overline{\emptyset} + \emptyset' \tag{1}$$

Likewise, for velocity:

$$u_i = \bar{u}_i + u_i' \tag{2}$$

where $\bar{u}_i$ and u_i' are mean and fluctuating velocity respectively (i = 1, 2, 3).

The continuity and momentum equations called Reynolds-average Navier-Stokes (RANS) in turbulent circumstance are written as follows equations respectively.

$$\frac{\partial \rho}{\partial t} + \frac{\partial}{\partial x_i}(\rho u_i) = 0 \tag{3}$$

$$\frac{\partial}{\partial t}(\rho u_i) + \frac{\partial}{\partial x_j}(\rho u_i u_j) = -\frac{\partial p}{\partial x_i} + \frac{\partial}{\partial x_j}\left[\mu\left(\frac{\partial u_i}{\partial x_j} + \frac{\partial u_j}{\partial x_i} - \frac{2}{3}\delta_{ij}\frac{\partial u_l}{\partial x_l}\right)\right] + \frac{\partial}{\partial x_j}(-\rho\overline{u_i' u_j'}) \tag{4}$$

Also, energy transfer due to conduction, species diffusion and viscous dissipation is:

$$\frac{\partial}{\partial t}(\rho E) + \nabla \cdot \left(\vec{V}(\rho E + p)\right) = \nabla \cdot \left(k_{eff}\nabla T - \sum_j h_j \vec{J}_j + (\bar{\tau}_{eff} \cdot \vec{V})\right) + S_h \tag{5}$$

where k_{eff} is effective conductivity and $\vec{J}_j$ is diffusion flux of species j.

On the right hand side of Eq. (5), the first three terms represent energy transfer due to conduction, species diffusion and viscous dissipation respectively and S_h is a combination of heat chemical reactant and every other heat resource which are defined.

Second-order discretization scheme is applied to solve all governing equations. The residual of the energy equation should drop below 10^{-6} and for all other variables it is set at 10^{-3} to ensure the convergence of the solution. The swirl velocity of components is eliminated in this steady-state CFD study. To investigate various aspects of biogas flameless combustion, the simulation is done in stoichiometric equivalence ratios (Φ = 1) and the results are compared by conventional combustion. Equivalence ratio is applied to show quantitatively whether the fuel–air in a chemical reaction is lean (Φ < 1), stoichiometric (Φ = 1) or rich (Φ > 1) [41]. The density of biogas consists of 60% CH_4 and 40% CO_2 in 300 K is considered 1.106 Kg/m^3. Table 1 demonstrates the densities of preheated air for different temperatures and various mixtures of N_2 and O_2.

The global combustion reaction of biogas, based on a different mole fraction of CO_2 is presented in Eq. (6) [42].

$$(1-\beta)[CH_4 + (2+x)(O_2 + 3.76N_2)] + \beta CO_2 \rightarrow CO_2 + 2(1-\beta) + H_2O + 7.56(1-\beta)N_2 + x(1-\beta)(O_2 + 3.76N_2) \tag{6}$$

Which x is the percentage of excess air and β is the mole fraction of CO_2 in biogas.

For biogas consist of 40% CO_2 and 60% CH_4, Eq. (2) can be written as Eq. (7).

$$0.6CH_4 + 0.4CO_2 + 1.2(O_2 + 3.76N_2) \rightarrow CO_2 + 1.2H_2O + 4.512N_2 \tag{7}$$

Based on a two step model developed by Westbrook and Dryer et al. [43] (WD model) for CH_4 combustion, the model consists of two following chemical reactions.

$$CH_4 + 3/2O_2 \rightarrow CO + 2H_2O \tag{8}$$

$$CO + 1/2O_2 \leftrightarrow CO_2 \tag{9}$$

In the chemical reaction (8), carbon monoxide (CO) and water vapor (H_2O) are formed, while in the chemical reaction (9) oxidation of CO to CO_2 and its dissociation takes place. This WD reduced model illustrates CO, CO_2 and H_2O formation. A chemical mechanism for combustion chemistry modeling has at least three parts: gas phase kinetic file (a list of all chemical reactions of interest to simulation including appropriate Arrhenius), thermodynamic data base (consist of thermodynamic coefficients for all gas phase kinetic file) and transport data file. The coefficient used for Eqs. (8) and (9) are values of Arrhenius equation coefficients.

$$k_{fi} = A_i T^{B_i} \exp\left(\frac{-E_i}{R_c T}\right) \tag{10}$$

where A_i is pre-exponential factor (for Eq. (8), it is equal to 2.8E+9 and for Eq. (9) it is 10.00E+14), βi is temperature coefficient (equal zero for both Eqs. (8) and (9)) and E_i is activation energy (for Eq. (8), it is equal to 48.4 and for Eq. (9) it is 40).

Table 1
The density (kg/m^3) of diluted air in various temperatures.

Temperature (K)	5%O_2	7%O_2	10%O_2	15%O_2	21%O_2
300	1.146	1.15	1.154	1.162	1.177
400	0.859	0.862	0.866	0.8717	0.8829
500	0.687	0.689	0.692	0.6973	0.7063
600	0.573	0.575	0.577	0.5811	0.5886
700	0.491	0.492	0.4946	0.4981	0.5046
800	0.429	0.431	0.433	0.4358	0.4415
900	0.382	0.383	0.3847	0.3874	0.3925
1000	0.344	0.345	0.3462	0.3486	0.3532
1100	0.312	0.313	0.3147	0.3169	0.3211
1200	0.286	0.287	0.2885	0.2905	0.2944

Presented gas phase kinetic file with thermodynamic data base and transport data file were applied for further simulation as reduced WD chemical reaction mechanism.

The Reynolds-averaged from of the governing equation is applied in conjunction with a turbulence model. For turbulent kinetic energy (k) and its dissipation (ε), the standard k–ε formulation is considered because of its accuracy and robustness for a wide range of turbulent flows. Indeed, since the k–ε model is valid for fully turbulent flow in CFD modeling and turbulence condition is effective in flameless combustion formation inside the chamber, this model could increase the accuracy of the calculations [44]. The thermal conductivity, specific heat and viscosity are computed with respect to the average of species mass fraction. Since the length of the chamber is longer than the molecular mean-free path of the reactants flowing through the chamber, Navier-Stokes equations are valid in the simulation. Radiation heat transfer between furnace inner walls is taken into account. A radiative transfer equation is solved for discrete solid angles across the numerical domain. Also, spatial variation in the total emissivity is calculated as a function of biogas composition and temperature because the weighted sum of the gray gas model (WSGGM) is incorporated. In WSGGM the total emissivity is considered as a function of the H_2O and CO_2 temperature and local mass fractions. The heat transfer radiation for spectral intensity for position $\vec{r}$ in direction $\vec{s}(I_\lambda(\vec{r},\vec{s}))$ is:

$$\nabla\cdot(I_\lambda(\vec{r},\vec{s}),\vec{s})+(a_\lambda+\sigma_s)I_\lambda(\vec{r},\vec{s}) = a_\lambda n^2 I_{b\lambda}+\frac{\sigma_s}{4\pi}\int_0^{4\pi} I_\lambda(\vec{r},\vec{s}')\Phi(\vec{s},\vec{s}')d\Omega' \quad (11)$$

Since simulation of radiation heat transfer from various thicknesses is possible by discrete ordinates (DO) model, surface-to-surface radiation heat transfer in the studied flameless combustor is modeled by DO. At the internal walls, non-slip and no species flux normal to the surfaces are considered. Moreover, heat loss from combustor surfaces to the surroundings is taken into account through Eq. (12) in which, both thermal heat transfer radiation and natural convection are accounted.

$$q=h(T_{s,o}-T_\infty)+\varepsilon\sigma(T_{s,o}^4-T_\infty^4) \quad (12)$$

where $T_{s,o}$ is the outer surface temperature, T_∞ is the ambient temperature set at 300 K, h is natural convection coefficient considered constant value 5 W/m^2 K, $\sigma = 5.67\times10^{-8}$ W/m^2 K^4 is Stephane-Boltzmann constant and ε is the solid surface emissivity.

The velocity distribution of the inlet oxidizer and fuel are uniform. The temperature of the inlet biogas is 300 K and the pressure outlet is 1.013×10^5 Pa. Eddy dissipation model (EDM) and volumetric reaction-based with respect to the two-step chemical kinetic mechanisms of biogas combustion is set. Therefore the application of an ignition source is not necessary to ignite the reactants and combustion proceeds in the presence of turbulence condition ($k/\varepsilon>0$). In the literature review it was stipulated that simulation of flameless combustion with EDC shows better results in the previous documents. However, in some cases, it has been mentioned that EDC is not appropriate for simulation. For instance Cristo and Dally et al. [32] pointed out that in some simulated cases EDC has overestimation. Damköhler number distribution (D_a), which represents the flow to chemical time-scale ratio could be effective for combustion model selection. Large Damköhler value indicates mixing controlled flames and low Damköhler value corresponds to slow chemical reactions. It means that reactants and products are quickly combined by turbulence and the combustion system behaves like a perfect stirred reactor. Therefore, calculation of the Damköhler number is required to set proper flow and chemical time-scales. The Damköhler (D_a) number characterizes the behavior between mixing and reaction in a system, given by the ratio of a mixing or flow time-scale to a chemical time-scale (τ_f/τ_c) [45]. Based Ref. [40], EDM is appropriate when $D_a>1$. Since in this study the distance between the centerline of fuel and oxidizer inlet is 52.5 mm, mixing time is long and chemical reaction time is short (due to biogas utilization) and D_a is greater than one. Thus, application of EDM shows acceptable results in this specific geometry. The radial inlet velocity of the oxidizer and fuel is negligible at the inlet of the furnace boundaries and the uniform axial velocities of biogas and oxidizer are set from the calculated biogas and oxidizer mass with respect to the density of the components. Turbulence intensity which is defined as Eq. (13) is set 10% and 20% for oxidizer and fuel respectively.

$$I=\frac{u'}{U} \quad (13)$$

where u' is the root-mean-square of the turbulent velocity fluctuations and U is the mean velocity in averaged Reynolds. In high turbulence models, turbulence intensity is considered 5–20% [46]. The dissipation rate inlet values of the turbulent kinetic energy are set based on the Versteeg and Malalasekera [47] applying the inner diameter of the biogas inlet and the hydraulic diameter of the oxidizer nozzle as characteristic lengths. For pressure-velocity coupling, coupled scheme is applied in solution methods and for other special discretization, second order upwind scheme is set. NO_x formation mechanisms include thermal NO_x and prompt NO_x were adopted based on the Ansys Fluent defaults. The transport equation for NO species formation is:

$$\frac{\partial}{\partial t}(\rho Y_{NO})+\nabla\cdot(\rho\vec{v}Y_{NO})=\nabla\cdot(\rho D\nabla Y_{NO})+S_{NO} \quad (14)$$

S_{NO} includes thermal NO_x determined by Zeldovich equations and prompt NO_x. Zeldovich equations are [48]:

$$O+N_2\leftrightarrow NO+N \quad (15)$$

$$N+O_2\leftrightarrow NO+O$$

$$N+OH\leftrightarrow NO+H$$

The reaction rate constants of aforementioned reactions are selected from Ref. [49] and partial equilibrium approach is taken into consideration to compute the concentration of OH and O radicals. The calculation of prompt NO_x formation is done from global model presented in Ref. [50].

$$CH+N_2\leftrightarrow HCN+N \quad (16)$$

$$N+O_2\leftrightarrow NO+O$$

$$HCN+OH\leftrightarrow CN+H_2O$$

$$CN+O_2\leftrightarrow NO+CO$$

The computed time averaged NO_x results is applied in Eq. (14). The computations were done by a core i7 computer with 16 GB of RAM and the cases solved between the parallel cores.

5. Results and discussion

5.1. Heat up

In order to achieve flameless mode, the furnace should be heated up at the first step and inside temperature of the chamber should increase over the auto-ignition of biogas. Fig. 4 displays the volumetric temperature distribution in conventional combustion of the pure CH_4 and biogas. Also, the variation of temperature on the centerline of the furnace fueled by CH_4 and biogas is demonstrated in this figure. The distribution of the temperature inside the chamber confirms that biogas is not eligible to be applied for heating up process practically. In the other word, biogas conventional

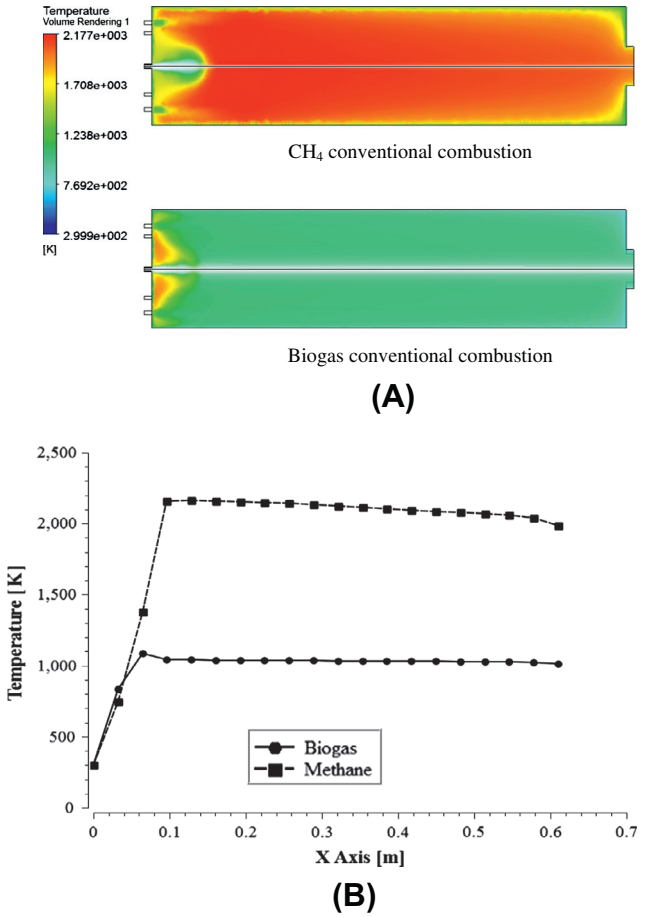

Fig. 4. (A) Temperature distribution in conventional combustion of the CH_4 and biogas. (B) Variation of temperature on the centerline of the furnace.

combustion cannot generate high temperatures inside the furnace. Therefore, in order to achieve flameless mode, furnace should be heated up by a high calorific value fuel such as CH_4.

5.2. Biogas conventional combustion with preheated air

The mean temperature of conventional preheated combustion increases inside the chamber due to high enthalpy of preheated air, consequently fuel consumption reduces drastically. Fig. 5 illustrates the effects of preheated air temperature on the fuel consumption in conventional combustion.

Although, preheated conventional combustion could be useful in fuel consumption minimization, NO_x formation increases in highly preheated combustion. This phenomenon is attributed to augmentation of the peak temperature in the furnace, because thermal NO_x intensifies sharply in high temperatures [17]. Fig. 6 shows the variation of peak temperature inside the furnace and NO_x formation in conventional preheated combustion with respect to the preheated oxidizer temperature. From this figure, it can be concluded that preheated conventional combustion of biogas cannot increase the inside temperature of the furnace significantly. However, conspicuous variation can be seen in the maximum temperature and NO_x formation in CH_4 preheated conventional combustion.

5.3. Flameless combustion

In this simulation, the concentration of oxygen in oxidizer is considered 5%, 7%, 10% and 15% by volume respectively and it is

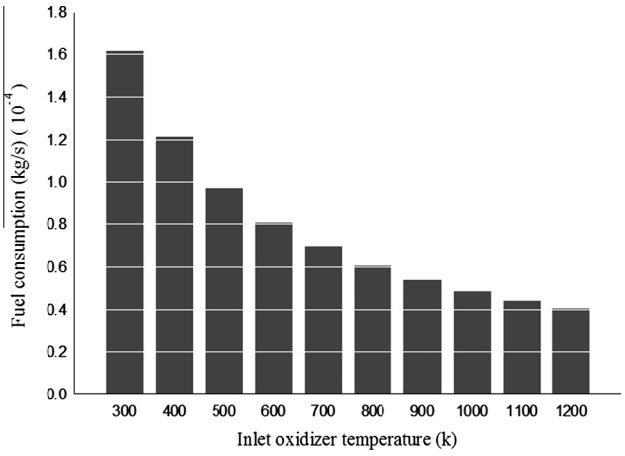

Fig. 5. The effects of preheated air temperature on the fuel consumption in conventional combustion.

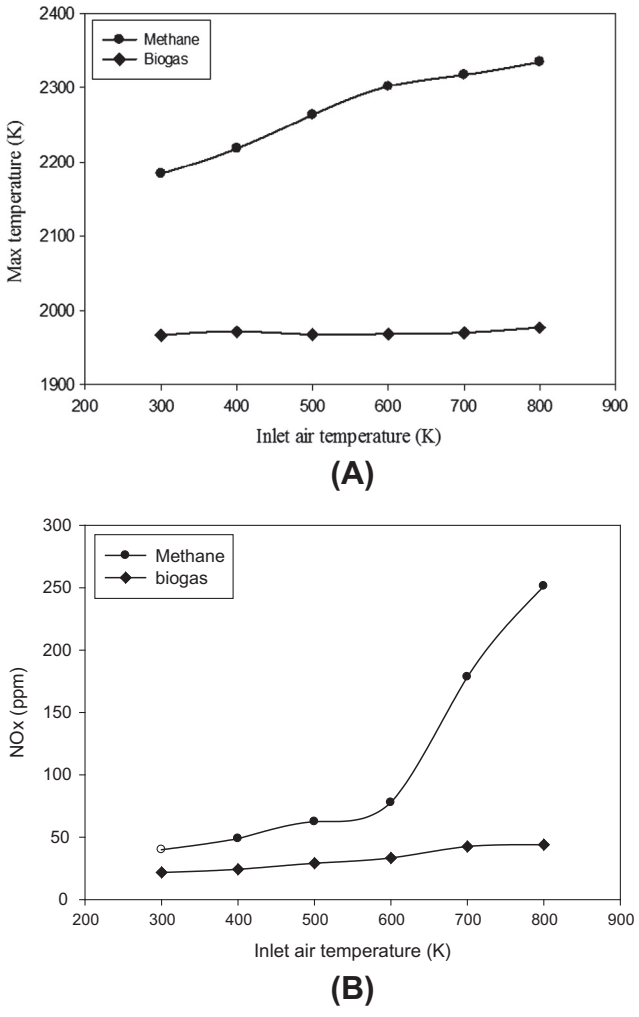

Fig. 6. (A) The variation of peak temperature in conventional preheated combustion. (B) NO_x formation in conventional preheated combustion.

assumed that oxidizer is diluted by N_2. Fig. 7 demonstrates the flameless constitution in the furnace when $V_{\text{inlet-air}} = 30$ m/s, $T_{\text{inlet-oxidizer}} = 900$ K and $\Phi = 1$.

Our experimental observations confirm that a small flame is constitute when oxygen concentration in oxidizer increased upto

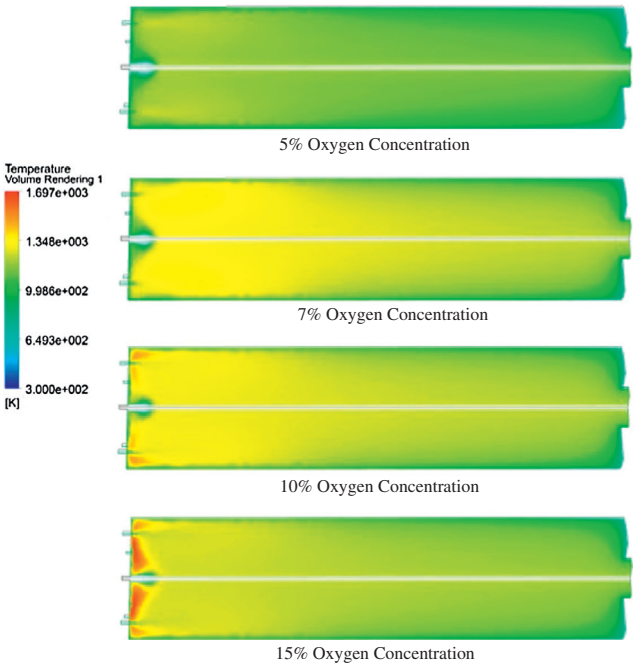

Fig. 7. Biogas flameless combustion formation with respect to the various oxygen concentrations.

15%. The maximum enthalpy in biogas flameless combustion is recorded 648,253 J/Kg but in conventional combustion the maximum enthalpy is 48,089 J/Kg. It can be construed that required enthalpy for biogas auto-ignition temperature is supplied by preheated oxidizer. In biogas flameless combustion, the mean temperature of the furnace is lower than CH_4 traditional combustion throughout the chamber. Compared to the biogas flameless combustion with uniform temperature, very high and fluctuated temperatures are recorded in conventional combustion. Consequently, hot spots which play crucial role in NO_x formation are eliminated in flameless mode. Since CO_2 constitutes 40% of biogas components, the temperature of the reactants decreases. It can be attributed to CO_2 high heat capacity especially in high temperatures [39]. The temperature inside the biogas flameless furnace is uniform averagely 1090 K. Also, wall temperature is lower and more uniform in flameless regime compared to the conventional mode. Fig. 8 shows the distribution of wall temperature in conventional and flameless regimes.

Based on mathematic formula of temperature uniformity ratio defined by Yang et al. [51], the ratio of uniformity in the flameless furnace is calculated around zero. This condition not only increases the durability of the refractory inside the chamber but also provides an ideal circumstance for NO_x formation reduction. Furthermore, fuel consumption decreases from 3.24 g/s in biogas conventional combustion to 1.07 g/s in flameless mode. Fig. 9 compared the entropy generation in centerline of the furnace in traditional and flameless combustion. Since high entropy generation intensifies irreversibility, exergy loss is higher in conventional combustion. Som and Datta [52] pointed out that the most irreversibility in a combustion system is related to the internal heat transfer within the combustor between the products and reactants. Chen et al. [53] stipulated that in the high temperature air combustion the irreversibility is attributed to the heat transfer in the reaction zones, however in the flameless mode, the reaction zones are dominated by the irreversibility due to chemical reaction. Entropy generation minimization in flameless mode could be attributed to the uniform temperature inside the chamber.

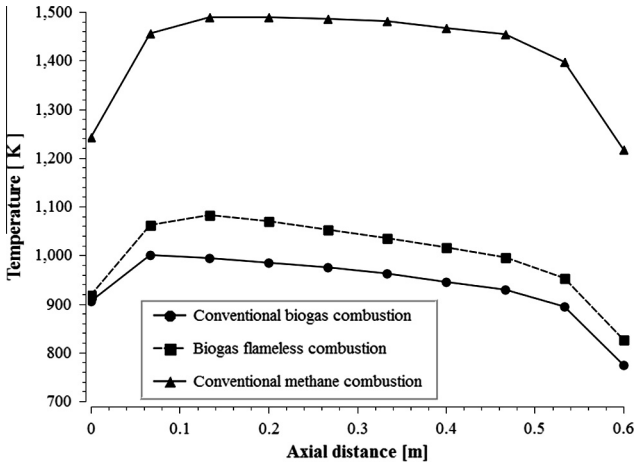

Fig. 8. Wall temperature distribution.

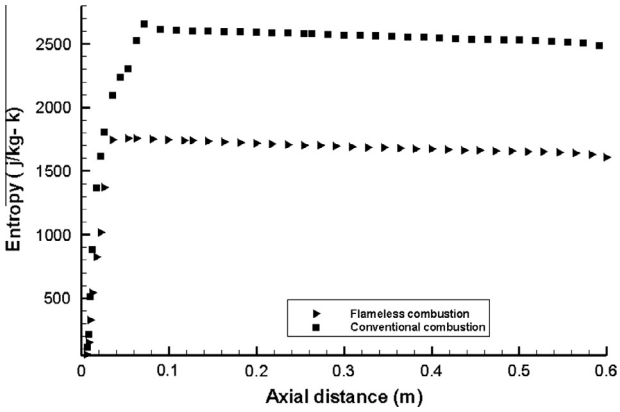

Fig. 9. Entropy generation in the furnace.

5.4. Species concentration in biogas flameless chamber

Fig. 10 demonstrates concentration of CH_4 and CO_2 along the central axis of the biogas flameless furnace. Since CH_4 and CO_2 form 60% and 40% of biogas respectively, the concentration of these species is very high at the entrance of the chamber. However, the concentrations of CH_4 and CO_2 decrease sharply in biogas flameless mode compared to the conventional combustion. It means that combustion phenomena takes place thorough the furnace homogeneously in flameless mode.

The streamline of the species in both conventional and flameless mode is shown in Fig. 11. The species of biogas are pulled to the oxidizer streamline due to various pressures. Since the velocity of the oxidizer is more than biogas, the vacuum circumstance causes the biogas species to be mixed with oxidizer. The mixture of the fuel and oxidizer species in flameless regime is done sooner than conventional mode due to the turbulence environment. In the other word, the complete biogas combustion occurred in the zone close to the burner.

Fig. 12 confirms that the concentration of O_2 along the furnace is very low and uniform. The low concentration of O_2 can be attributed to diluted oxidizer and the complete and quick mixing process in biogas flameless mode. Apart from that, the uniform temperature inside the flameless chamber which is higher than the biogas self-ignition temperature guarantees the stable conditions for the biogas flameless regime formation. The high amount of CO concentration in flameless regime is attributed to low OH

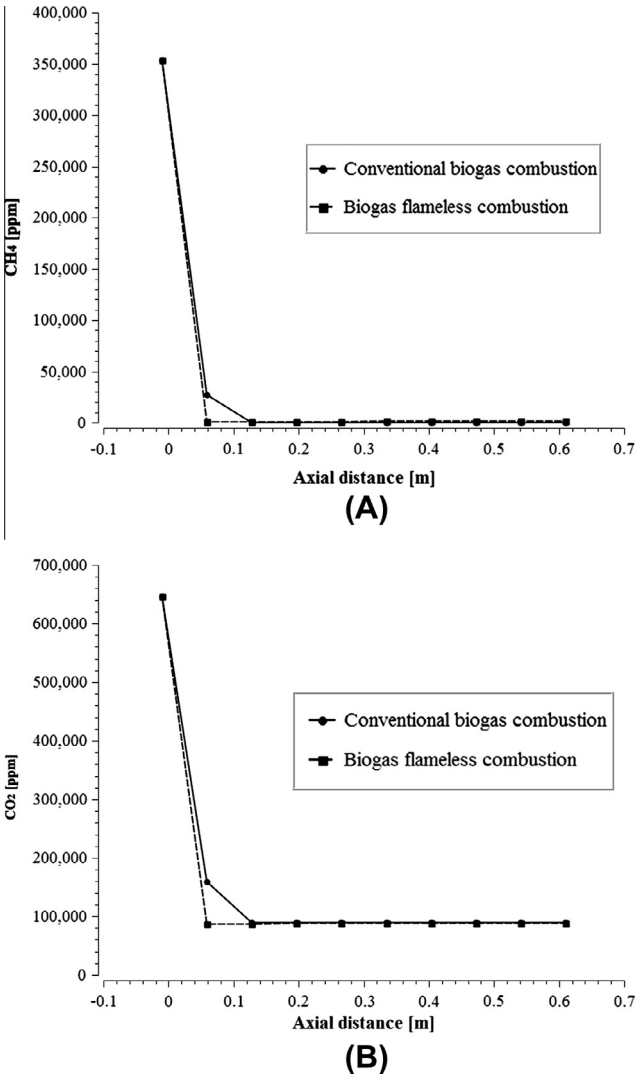

Fig. 10. Concentration of CH_4 and CO_2 along the central axis of the furnace.

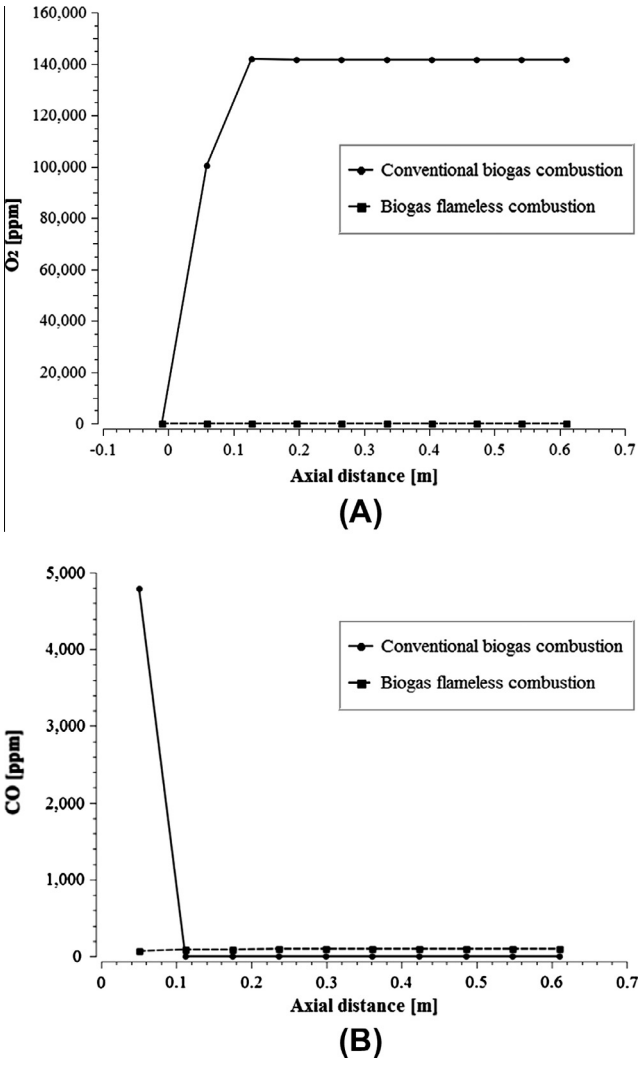

Fig. 12. (A) Oxygen concentration and (B) monoxide carbon concentration pattern inside the furnace.

radical concentration which controls the CO conversion to CO_2 [54].

Fig. 13 depicts NO_x formation pattern along the chamber. The constitution of NO_x is very low in flameless mode. However, in conventional combustion of CH_4 and biogas the NO_x emission in the outlet of the chamber was recorded 45 ppm and 22 ppm respectively. The low level of NO_x formation in flameless combustion is attributed to uniform low temperature in flameless mode. In the other hand, the very high temperature of the flame in traditional combustion is responsible for high level of thermal NO_x formation. Simulated results confirm that thermal NO_x formation is eliminated in low temperature flameless combustion, and NO_x formation occurs via N_2O-intermediate model.

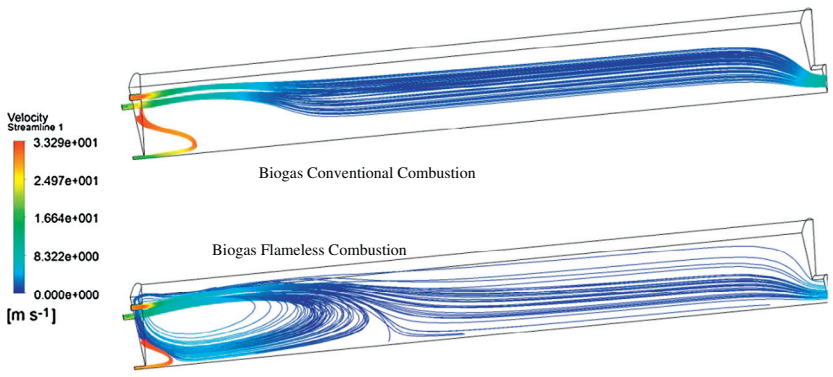

Fig. 11. The streamline of the species.

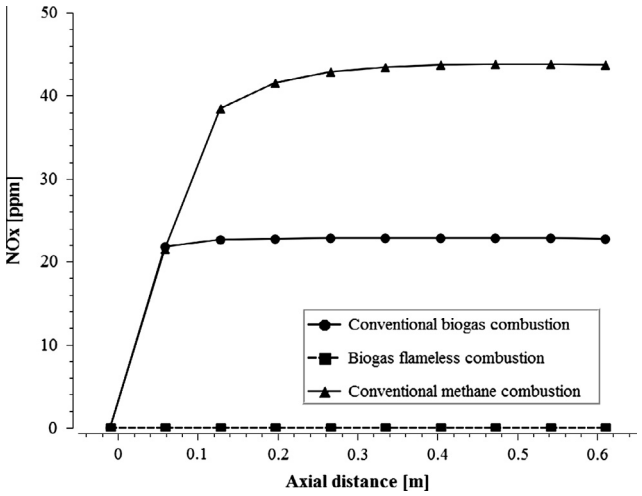

Fig. 13. NO_x formation in the furnace.

6. Conclusion

Computational fluid dynamic investigation was performed to analyze combustion characteristics of biogas flameless regime. The two-step reaction scheme was simulated with EDM and the standard k–ε formulation was applied due to its accuracy and robustness for wide range of turbulent flows. Surface-to-surface radiation heat transfer was modeled by DO due to its great ability in simulation of various thicknesses. Due to elimination of ignition in biogas flameless mode, the required enthalpy for biogas auto-ignition temperature is supplied by enthalpy of preheated oxidizer. The effects of preheated temperature on conventional combustion were discussed. It was found that in preheated biogas conventional combustion, fuel consumption decreases however NO_x formation increases drastically. Indeed, the differences between reactants and products temperature could intensify irreversibility in traditional combustion. Since the temperature inside the chamber as well as wall temperature is uniform in biogas flameless mode exergy loss decreases in flameless combustion technique. Indeed, NO_x formation reduces in flameless mode due to elimination of hot spots and low level of oxygen. The streamline of the species in both conventional and flameless mode indicate that the species of biogas are pulled to the oxidizer streamline due to various pressures. The mixture of the fuel and oxidizer species in flameless regime is done faster than conventional mode due to the turbulence environment and complete biogas combustion is projected in the zone close to the burner. Also, low concentration of O_2 in the flameless mode is attributed to dilution of oxidizer and the complete and quick mixing process. Indeed, very high concentration of CO_2 species in biogas flameless products causes higher heat capacity and better radiation heat transfer in the system.

References

[1] Hosseini Seyed Ehsan, Wahid MA. Necessity of biodiesel utilization as a source of renewable energy in Malaysia. Renew Sustain Energy Rev 2012;16(8):5732–40.
[2] Makareviciene Violeta, Sendzikiene Egle, Pukalskas Saugirdas, Rimkus Alfredas, Vegneris Ricardas. Performance and emission characteristics of biogas used in diesel engine operation. Energy Convers Manage 2013;75:224–33.
[3] Hosseini Seyed Ehsan, Wahid MA, Aghili Nasim. The scenario of greenhouse gases reduction in Malaysia. Renew Sustain Energy Rev 2013;28:400–9.
[4] Colak Ilhami, Sagiroglu Seref, Demirtas Mehmet, Yesilbudak Mehmet. A data mining approach: analyzing wind speed and insolation period data in Turkey for installations of wind and solar power plants. Energy Convers Manage 2013;65:185–97.
[5] Zhou Cheng, Doroodchi Elham, Moghtaderi Behdad. An in-depth assessment of hybrid solar–geothermal power generation. Energy Convers Manage 2013;74:88–101.
[6] Hosseini Seyed Ehsan, Andwari Amin Mahmoudzadeh, Wahid Mazlan Abdul, Bagheri Ghobad. A review on green energy potentials in Iran. Renew Sustain Energy Rev 2013;27:533–45.
[7] Demirbas Ayhan. Waste management, waste resource facilities and waste conversion processes. Energy Convers Manage 2011;52(2):1280–7.
[8] Corro Grisel, Pal Umapada, Bañuelos Fortino, Rosas Minerva. Generation of biogas from coffee-pulp and cow-dung co-digestion: infrared studies of postcombustion emissions. Energy Convers Manage 2013;74:471–81.
[9] Rasi S, Läntelä J, Rintala J. Trace compounds affecting biogas energy utilisation – a review. Energy Convers Manage 2011;52(12):3369–75.
[10] Hosseini Seyed Ehsan, Wahid MA. Feasibility study of biogas production and utilization as a source of renewable energy in Malaysia. Renew Sustain Energy Rev 2013;19:454–62.
[11] Taleghani G, Shabani Kia A. Technical–economical analysis of the Saveh biogas power plant. Renew Energy 2005;30:441–6.
[12] Hosseini, Ehsan Seyed, Wahid Mazlan A, Abuelnuor Abuelnuor Abdeen Ali. Biogas flameless combustion: a review. Appl Mech Mater 2013;388:273–9.
[13] Flamme Michael. Low NOx combustion technologies for high temperature applications. Energy Convers Manage 2001;42(15):1919–35.
[14] Choi Gyung-Min, Katsuki Masashi. Advanced low NO_x combustion using highly preheated air. Energy Convers Manage 2001;42(5):639–52.
[15] Hosseini Seyed Ehsan, Wahid MA, Abuelnuor AAA. Pollutant reduction and energy saving in industrial sectors by applying high temperature air combustion method. Int Rev Mech Eng 2012;6(7):1667–72.
[16] Hosseini Seyed Ehsan, Salehirad Saber, Wahid MA, Sies Mohsin Mohd, Saat Aminuddin. Effect of diluted and preheated oxidizer on the emission of methane flameless combustion. In: AIP conference proceedings, vol. 1440; 2012. p. 1309.
[17] Hosseini Seyed Ehsan, Wahid MA, Abuelnuor AAA. High temperature air combustion: sustainable technology to low NOx formation. Int Rev Mech Eng 2012;6(5):947–53.
[18] House, David. The complete biogas handbook. Alternative House Information; 2010.
[19] Bedoya Iván D, Saxena Samveg, Cadavid Francisco J, Dibble Robert W, Wissink Martin. Experimental study of biogas combustion in an HCCI engine for power generation with high indicated efficiency and ultra-low NOx emissions. Energy Convers Manage 2012;53(1):154–62.
[20] Tsuji Hiroshi, Gupta Ashwani K, Hasegawa Toshiaki, Katsuki Masashi, Kishimoto Ken, Morita Mitsunobu. High temperature air combustion: from energy conservation to pollution reduction. CRC Press; 2010.
[21] Rebola A, Coelho PJ, Costa M. Assessment of the performance of several turbulence and combustion models in the numerical simulation of a flameless combustor. Combust Sci Technol 2013;185(4):600–26.
[22] Weber Roman, Orsino Stefano, Lallemant Nicolas, Verlaan AD. Combustion of natural gas with high-temperature air and large quantities of flue gas. Proc Combust Inst 2000;28(1):1315–21.
[23] Mancini Marco, Weber Roman, Bollettini Ugo. Predicting NOx emissions of a burner operated in flameless oxidation mode. Proc Combust Inst 2002;29(1):1155–63.
[24] Orsino Stefano, Weber ROMAN, Bollettini Ugo. Numerical simulation of combustion of natural gas with high-temperature air. Combust Sci Technol 2001;170(1):1–34.
[25] Mancini Marco, Schwöppe Patrick, Weber Roman, Orsino Stefano. On mathematical modelling of flameless combustion. Combust Flame 2007;150(1):54–9.
[26] Kim Ju Pyo, Schnell Uwe, Scheffknecht Günter. Comparison of different global reaction mechanisms for mild combustion of natural gas. Combust Sci Technol 2008;180(4):565–92.
[27] Coelho PJ, Peters N. Numerical simulation of a mild combustion burner. Combust Flame 2001;124(3):503–18.
[28] Dally Bassam B, Riesmeier E, Peters N. Effect of fuel mixture on moderate and intense low oxygen dilution combustion. Combust Flame 2004;137(4):418–31.
[29] Khoshhal Abbas, Rahimi Masoud, Alsairafi Ammar Abdulaziz. CFD study on influence of fuel temperature on NOx emission in a HiTAC furnace. Int Commun Heat Mass Transfer 2011;38(10):1421–7.
[30] Wunning JA, Wunning JG. Prog Energy Combust Sci 1997;23:81–94.
[31] Weber R, Verlaan AL, Orsino S, Lallemant N. J Inst Energy 1999;72:77–83.
[32] Christo FC, Dally Bassam B. Modeling turbulent reacting jets issuing into a hot and diluted coflow. Combust Flame 2005;142(1):117–29.
[33] Galletti Chiara, Parente Alessandro, Tognotti Leonardo. Numerical and experimental investigation of a mild combustion burner. Combust Flame 2007;151(4):649–64.
[34] Parente Alessandro, Galletti C, Tognotti L. A simplified approach for predicting NO formation in MILD combustion of CH4/H2 mixtures. Proc Combust Inst 2011;33(2):3343–50.
[35] Schütz H, Lückerath R, Kretschmer T, Noll B, Aigner M. Analysis of the pollutant formation in the FLOX combustion. J Eng Gas Turb Power 2008;130(1).
[36] Danon B, De Jong W, Roekaerts DJEM. Experimental and numerical investigation of a FLOX combustor firing low calorific value gases. Combust Sci Technol 2010;182(9):1261–78.

[37] Chen Sheng, Zheng Chuguang. Counterflow diffusion flame of hydrogen-enriched biogas under MILD oxy-fuel condition. Int J Hydrogen Energy 2011;36(23):15403–13.
[38] Gassoumi T, Guedri K, Said R. Numerical study of the swirl effect on a coaxial jet combustor flame including radiative heat transfer. Numer Heat Transfer A 2009;56(11):897–913.
[39] Hosseini Seyed Ehsan, Wahid MA. Biogas utilization: *experimental investigation on biogas flameless combustion in lab-scale furnace*. Energy Convers Manage 2013;74:426–32.
[40] Fluent Ansys. 14.0 Theory Guide. Ansys Inc., vol. 5; 2012.
[41] Turns SR. An introduction to combustion. New York: McGraw-Hill; 1996.
[42] Cohé Cécile, Chauveau Christian, Gökalp Iskender, Kurtuluş Dilek Funda. CO_2 addition and pressure effects on laminar and turbulent lean premixed CH_4 air flames. Proc Combust Inst 2009;32(2):1803–10.
[43] Westbrook Charles K, Dryer Frederick L. Simplified reaction mechanisms for the oxidation of hydrocarbon fuels in flames. Combust Sci Technol 1981;27(1–2):31–43.
[44] Wilcox David C. Turbulence modeling for CFD, vol. 2. La Canada: DCW Industries; 1998.
[45] Isaac Benjamin J, Parente Alessandro, Galletti Chiara, Thornock Jeremy N, Smith Philip J, Tognotti Leonardo. A novel methodology for chemical time scale evaluation with detailed chemical reaction kinetics. Energy Fuels 2013;27(4):2255–65.
[46] http://www.cfd-online.com/.
[47] Versteeg HK, Malalasekera W. An introduction to computational fluid dynamics: the finite volume method, 2/E. Pearson Education; 2007.
[48] Bowman C. Kinetics of pollutant formation and destruction in combustion. Prog Energy Combust Sci 1975;1:33–45.
[49] Hanson Ronald K, Salimian Siamak. Survey of rate constants in the N/H/O system. Combustion chemistry. US: Springer; 1984. p. 361–21.
[50] DS, GG. Overall reaction rates of NO and N_2 formation from fuel nitrogen. Pittsburg, PA, USA: The Combustion Institute; 1974. p. 1093.
[51] Yang Weihong, Blasiak Wlodzimierz. CFD as applied to high temperature air combustion in industries furnaces. IRFR Combust J; November 2006.
[52] Som SK, Datta A. Thermodynamic irreversibilities and exergy balance in combustion processes. Prog Energy Combust Sci 2008;34(3):351–76.
[53] Chen Sheng, Mi Jianchun, Liu Hao, Zheng Chuguang. First and second thermodynamic-law analyses of hydrogen-air counter-flow diffusion combustion in various combustion modes. Int J Hydrogen Energy 2012;37(6):5234–45.
[54] Szegö GG, Dally BB, Nathan GJ. Operational characteristics of a parallel jet MILD combustion burner system. Combust Flame 2008;156:429–38.